Experimental study of smectite interaction with metal iron at low temperature: 1. Smectite destabilization.

Sébastien Lantenois, Bruno Lanson, Fabrice Muller, Andreas Bauer, Michel Jullien, Alain Plançon

Experimental study of smectite interaction with metal iron at low temperature: 1. Smectite destabilization.

Sébastien Lantenois[(1)] *, Bruno Lanson[(2)], Fabrice Muller[(1)], Andreas Bauer[(3)], Michel Jullien[(4)], Alain Plançon[(1)]

(1) Institut des Sciences de la Terre d'Orléans (ISTO), CNRS – Université d'Orléans, 1A rue de la Férollerie, 45071 Orléans Cedex 2, France.

(2) Environmental Geochemistry Group, LGIT, Maison des GéoSciences, Université J. Fourier – CNRS, BP 53, 38041 Grenoble Cedex 9, France.

(3) Institut für Nukleare Entsorgung, Forschungzentrum Karlsruhe, P.O. Box 3640, 76021 Karlsruhe Germany.

(4) Commissariat à l'Energie Atomique (CEA), Centre d'Etude de Cadarache DEN/DTN/SMTM/Laboratoire de Modélisation des Transferts dans l'Environnement , Bat 307, 13108 Saint Paul Lez Durance Cedex, France.

* Author to whom correspondence should be addressed.

e-mail: sebastien.lantenois@univ-orleans.fr

KEYWORDS: nuclear waste disposal, engineered barrier, clay barrier, iron-clay interactions, iron corrosion, clay stability, X-ray diffraction, smectite.

ABSTRACT

Interaction between metal iron and a variety of natural and synthetic smectites samples with contrasting crystal chemistry was studied by scanning electron microscopy and X-ray diffraction (XRD) from experiments conducted at 80°C. These experiments demonstrate an important reactivity contrast as a function of smectite crystal chemistry. An XRD quantification method involving the use of an internal standard allowed quantification of the relative proportion of smectite destabilized as a function of initial pH conditions as well as of smectite structural parameters. In mildly acidic to neutral pH conditions, a significant proportion of metal iron is corroded to form magnetite without smectite destabilization. Under basic pH conditions, smectite and metal iron are partly destabilized to form magnetite and newly-formed 1:1 phyllosilicate phases (odinite and crondstedtite). Systematic destabilization of both metal iron and smectite is observed for dioctahedral smectites while trioctahedral smectites are essentially unaffected under similar experimental conditions. Smectite reactivity is enhanced with increasing Fe^{3+} content and with the presence of Na^{+} cations in smectite interlayers. A conceptual model for smectite destabilization is proposed. This model involves first the release of protons from smectite structure, $MeFe^{3+}OH$ groups being deprotonated preferentially and metal iron acting as proton acceptor. Corrosion of metal iron results from its interaction with these protons. Fe^{2+} cations resulting from this corrosion process sorb on the edges of smectite particles and lead to induce the reduction of structural Fe^{3+} and migrate into smectite interlayers to compensate for the increased layer charge deficit. Interlayer Fe^{2+} cations subsequently migrate to the octahedral sheet of smectite because of the extremely large layer charge deficit. At low temperature, this migration is favored by the reaction time and by the absence of protons within the di-trigonal cavity. Smectite destabilization results

from the inability of the tetrahedral sheets to accommodate the larger dimensions of the newly formed trioctahedral domains resulting from the migration of Fe^{2+} cations.

INTRODUCTION

In some of the "multi-barriers" concepts envisaged for the storage of high- and intermediate-level and/or long-lived nuclear waste, metallic containers filled with vitrified nuclear waste are placed in a confinement barrier itself surrounded by a geological barrier. The reactive components of the engineered and geological barriers are clays (mainly smectites) while metallic containers could be made up of iron. To predict the long-term properties of these clay barriers, it is thus essential to study the interactions between clay minerals, and more especially smectite, and metal iron as the corrosion of the metallic canister could induce in turn the destabilization of the clay minerals.

Studies of these iron-clay interactions have shown indeed the partial but systematic destabilization of the initial clay material and the subsequent crystallization of reaction products (Habert, 2000; Perronnet, 2001, 2004; Kohler, 2001; Lantenois, 2003; Guillaume *et al.,* 2003). The nature of these reaction products depends on experimental conditions such as temperature and, to a minor extent, the nature of the initial clay material. When smectite is used, iron-rich chlorite-like species are synthesized at high temperature (300°C - Guillaume *et al.,* 2003) whereas iron-rich serpentine-like species are obtained for temperatures more realistic in the context of nuclear waste disposal (80°C - Habert, 2000; Perronnet, 2001, 2004; Lantenois, 2003). Newly formed 1:1 phyllosilicates with low iron content were also identified by Kohler (2001) after reaction between iron metal and kaolinite/smectite mixtures at 80°C.

As reaction pathways appear to vary significantly as a function of temperature (Guillaume *et al.*, 2003; Lantenois, 2003), it is especially important to work at temperatures similar to those expected during storage lifetimes, thus generally excluding medium-to-high temperature experiments (>200°C). Experimental conditions have been chosen to mimic those of the repository, and experiments were thus performed in an anoxic and reducing

environment. The clay materials used for this study were essentially natural smectites which have swelling and self-healing abilities and cation retention properties suitable for engineered barriers. To promote the reactivity of clays so that significant reaction progress could be obtained on a laboratory-compatible timescale, the water/solid ratio was significantly increased.

A method has been developed to quantify the amount of smectite destabilized as a result of its interaction with metal iron. The aim of the present study was to determine the role of the nature of clay minerals on the contrasting reactivity observed during their hydrothermal reaction with iron metal by using a variety of starting materials. Specifically, the structural characteristics responsible for these differences were sought, together with the mechanism of clay destabilization. The companion paper (Lantenois *et al.*, 2005) will describe the crystal-chemistry of newly-formed phases.

MATERIALS AND METHODS

Materials

A variety of natural and synthetic smectite samples with contrasting crystal chemistry were used in the present study. These samples were selected to include both di- and trioctahedral varieties, smectite with octahedral or tetrahedral substitutions, and to cover a wide range of chemical composition, focusing on the iron content. Chemical compositions of selected samples are reported in Table 1. Untreated bulk samples were ground in an agate mortar to increase their reactivity, but samples were neither size-fractionated nor purified.

Synthetic clays were crystallized from gels under hydrothermal conditions. Gels were prepared following a method adapted from Hamilton and Henderson (1968) using tetraethyl

orthosilicate (TEOS), $Mg(NO_3)_2.6H_2O$, $Al(NO_3)_3.9H_2O$, $Fe(NO_3)_3.9H_2O$, HNO_3, Na_2CO_3, NH_4OH and ethanol. All reagents had a 99% minimum grade. After dissolution of Al- and Mg-nitrates and of Na_2CO_3 in nitric acid, TEOS and ethanol were added. A precipitate was obtained by neutralizing the resulting solution at pH ~ 6 with addition of NH_4OH. This precipitate was dried at 80°C for 24 hours, ground in an agate mortar and heated to 400°C to remove nitrates and carbonates and to obtain a gel composed essentially of Al, Mg, Si and Na oxides. SapFe08 saponite was synthesized from such gels in a cold-sealed pressure vessel. Gel and deionized water were introduced in a 2:1 weight ratio in a silver tube itself placed in the vessel heated at 400°C for one month at an estimated pressure of 100 MPa (Suquet *et al.*, 1977). The SbS-1 beidellite was synthesized in an internally heated pressure vessel. 600 mg of gel were mixed to 1.3 g of a NaOH solution (0.2N) in a gold tube. The tube was then sealed and heated to 350°C under 22 MPa for 10 days (Kloprogge *et al.*, 1999). After cooling of the vessels, the solid products were extracted from the reaction tubes, dried at 80°C overnight, and ground before structural and chemical characterization using X-ray diffraction (XRD) and energy dispersive X-ray fluorescence spectroscopy (EDS) on a transmission electron microscope (TEM).

To better assess the role of the interlayer composition on the reaction rate K-, Na-, and Ca-saturated specimens were prepared for samples SWy-2, Garfield, and SAz-1. The cation exchange procedure was performed at room temperature by immersing the ground clay sample in 1M KCl, NaCl or $CaCl_2$ aqueous solutions. After 12 hours of contact, the solid was extracted by centrifugation. The saturation procedure was repeated four times. The excess chloride was then removed by washing the sample five times with distilled water (K- and Ca-saturated samples). Na-saturated samples were washed once in ethanol, and then dialysed in deionized water for one week.

123 *Experimental*

124

125 For the iron-clay interactions, 0.6 g of the clay powder were mixed with 0.6 g of metal
126 iron powder (10 μm maximum size, Merck® product for analysis) to maximize the contact
127 surface between iron and clay particles. The large amount of metal iron was intended also to
128 promote reducing conditions during the experiments. 30 mL of water were added to this
129 initial mixture. Deionized water (with a resistivity >18MΩ cm^{-1}) was used to allow studying
130 the final solution composition. Samples were prepared in a MBraun® glove box equipped with
131 copper catalysts to eliminate O_2, and a MBraun® O_2 control system. Partial pressure of O_2 was
132 lower than 1 ppm during sample preparation. Deionized water was degassed with Argon for
133 one hour prior to its introduction in the glove box and all products were allowed to stay in the
134 glove box for 24 hours to equilibrate with the glove box atmosphere. Starting products were
135 then placed in 40 mL Nalgene® reactors. Because these reactors are oxygen porous, a "double
136 enclosure system" was used where the Nalgene® reactors were inserted into larger Teflon®
137 reactors which contain metal iron powder, $FeSO_4$ and water. Any oxygen entering the Teflon
138 reactors was thus eliminated according to reactions (1) and (2) with ferrous and metal iron,
139 respectively (Aogaki, 1999).

140 $$2Fe^{2+} + 1/2O_2 + 3H_2O \rightarrow 4H^+ + 2FeOOH \quad (1)$$

141 $$2Fe^{\circ} + 3/2O_2 + 3H_2O \rightarrow 2Fe(OH)_3 \quad (2)$$

142 The two reactors were tightly closed within the glove box and subsequently heated at
143 80°C for 45 days outside of the glove box. Additional experiments were also performed for 5,
144 15, 30, 60, 90 and 120 days on selected samples (Garfield, SbId, SWy-2 and SapCa-2). At the
145 end of the reactions, reactors were cooled down to room temperature and opened in air, the
146 solution pH being measured immediately. The solution was subsequently filtered (0.45 μm)

147 and acidified for chemical analysis, whereas the solid fraction was dried at 80°C overnight
148 and ground.

149 Filtered solutions were analyzed for major and trace elements (Si, Al, Fe, Mg, Ti, Na,
150 Ca and K) with an ICP-AES Jobin-Yvon ULTIMA spectrometer. Scanning electron
151 microscopy (SEM) was performed using a JEOL 6400 microscope. Samples were covered
152 with a Au film before observation to avoid charge build up. TEM was performed using a
153 JEOL 2000 FX microscope operated at 200 kV. Samples were prepared as a suspension in
154 deionized water, a drop of this suspension being dried on copper grids covered with a carbon
155 film.

156 Powder XRD patterns were recorded in transmission geometry using CoKα radiation
157 (35 mA, 35 kV) to avoid iron fluorescence. The use of an INEL CPS 120 curved position
158 sensitive detector allowed recording simultaneously the diffracted intensity over a 4-50°2θ
159 range with a step size of 0.03°. The non-linearity of the detector was corrected (Roux and
160 Wolfinger, 1996). A 0.5 mm diameter Lindemann glass tube was used to hold the sample
161 powder.

162 Infrared (IR) spectra were recorded over the 650–4000 cm^{-1} range with a 2 cm^{-1}
163 resolution using a Nicolet Magna-IR Fourier transform spectrometer equipped with a Globar
164 SiC source and a DTGS detector. The spectrometer was purged with dry air prior to data
165 collection to remove most of atmospheric H_2O. The sample was finely ground in an agate
166 mortar, and 0.5 mg of the resulting powder was mixed to 150 mg of KBr previously dried at
167 120°C for 24 hours. The mixture was homogenized and pressed in an evacuable die to
168 prepare a 12 mm diameter pellet. Decomposition of the IR spectra in the OH bending region
169 (700 – 900 cm^{-1}) was performed with Peak-Fit (v4.05).

170 The cation exchange capacity (CEC) was measured using the copper complex method
171 (Gaboriau, 1991). 600 mg of sample were suspended for 12 hours in 25 mL of a 0.02 N

ethylene di-amine copper complex ($Cu(EDA)_2Cl_2$) solution. After centrifugation, the Cu concentration in solution was measured using a 905-GBC atomic absorption spectrophotometer from GBC Scientific Equipment.

Quantification of the relative proportion of smectite destabilized after reaction

To estimate reaction progress, the amount of residual smectite was quantified by XRD using the internal standard technique adapted to clays by Hillier (2000). As recommended by this author, each sample was mixed with 10% of a corundum internal standard (particle size < 50µm), dry ground in an agate mortar for 10 minutes and then introduced in the Lindeman glass tube. The use of a glass tube in transmission geometry allows optimizing sample disorientation. Segregation due to particle size and/or particle density was minimized by careful grinding and mixing. Absorption corrections have not been considered because absorption, which is closely related to sample chemical composition, is similar before and after reaction.

The (001) reflection of smectite was not selected for quantification, because its intensity strongly depends on smectite hydration state and thus on the chemical composition of smectite interlayers, which can be modified during the reaction. The amount of residual smectites was rather quantified by measuring the integrated intensity of the (02,11) band (between 22.0° and 27.0°2θ CoKα - Figure 1) before and after reaction, these intensities being normalized to the (012) reflection of corundum (29.8°2θ CoKα - Figure 1). Background was assumed to be linear between 22.0 and 27.0°2θ and subtracted. If quartz impurities were present, the (100) reflection of quartz (~24.3°2θ CoKα) was fitted, and its integrated intensity subtracted from the total integrated intensity. To assess the validity of XRD results, the relative proportion of reacted smectite was also quantified from CEC

197 measurements performed before and after reaction, the observed CEC decrease being directly
198 linked to the amount of destabilized smectite. This assumption was made possible by the non-
199 swelling character of the reaction products (Lantenois, 2003; Lantenois *et al.*, 2005).

200 The amount of residual smectite was also quantified using IR spectroscopy. Over the
201 OH bending frequency range, three bands at 912-920 cm^{-1}, 874-886 cm^{-1}, and 840-850 cm^{-1}
202 correspond to the Al-Al-OH, Al-Fe-OH and Al-Mg-OH vibrations of smectites, respectively
203 (Farmer, 1974; Goodman *et al.*, 1976; Russell and Fraser, 1994; Vantelon *et al.*, 2001). The
204 position reported in the literature for the Fe-Fe-OH band scatters from 820-795 cm^{-1}
205 (Goodman *et al.*, 1976; Cuadros and Altaner, 1998) and overlaps with the Si-O vibrations of
206 quartz at 780 and 800 cm^{-1} (Madejova and Komadel, 2001). To avoid using this problematic
207 band, reaction progress was quantified using IR spectroscopy for Fe-poor smectites only. The
208 quantification method itself requires subtracting a baseline which corresponds to Si-O
209 vibrations in phyllosilicates (Figure 2a – Vantelon *et al.*, 2001). A cubic spline baseline,
210 similar for all samples, was adjusted on both sides of the region of interest (817-822 cm^{-1} and
211 940-945 cm^{-1}, respectively). The 822-945 cm^{-1} range of the baseline-corrected spectra was
212 then fitted with three Gaussian-shaped curves (Figures 2b) corresponding to Al-Al-OH, Al-
213 Fe-OH and Al-Mg-OH vibration modes. Relative proportion of unaltered smectite was
214 estimated from the ratio between the total surface areas determined for these three
215 contributions before and after reaction.
216

RESULTS

Qualitative evaluation of the reaction progress

Long-term experiments show that the reaction progress reaches a plateau after about 30 days (see below). Except when specifically notified, reactions described in the following section were thus performed for 45 days, without constraining the solution pH. The observed reaction depends on the nature of the initial smectite sample. In particular di- and tri-octahedral smectites exhibit contrasting reactivities and will be described separately.

Dioctahedral smectites. Although reaction progress varies considerably as a function of the initial smectite sample, a similar effect was observed for all dioctahedral smectites. After 45 days, solution pH was not significantly modified, whereas the chemical composition of the solutions was altered (Table 2). In particular, the concentration in solution of alkali and alkali-earth cations which were initially present in smectite interlayers (Na^+, Ca^{2+}, and K^+) was significantly increased after reaction (Table 2) together with that of silicon. For smectite samples reacted without metal iron, Si was not detected in solution, and the concentration in solution of alkali and alkali-earth cations after reaction was lower than in similar experiments performed in presence of metal iron (Table 2). In all reacted samples residual metal iron was systematically present together with newly-formed phases (magnetite and 7 Å phyllosilicates – Figure 1a-e). However, iron particles observed in all reacted samples appear corroded as compared to their initial state (Figure 3a,b). In addition, clay particles with a distinct morphology were observed in all reacted samples (Figure 3c). These particles most likely correspond to the newly-formed phyllosilicate phase. Unreacted clay particles were also observed for both montmorillonite and beidellite samples (Figures 3d,e). Accordingly, residual smectite was identified for montmorillonite and beidellite samples from its (02,11)

band at ~23°2θ CoKα (Figure 1a-d). The intensity of this characteristic band was much reduced after reaction for Garfield nontronite sample (Figure 1e), in agreement with the absence of unreacted clay particles in the reacted Garfield sample (Figure 3f).

Trioctahedral smectites. For saponite samples, solution pH and composition are not significantly modified after 45 days of iron-clay interactions (Table 2). Accordingly, XRD patterns recorded on both unreacted and reacted samples are alike (Figure 1f). In particular, the (02,11) band (~23°2θ CoKα) is similar in both samples, an even the (001) reflection (~7°2θ CoKα) is practically unaffected. In addition, no extra reflection was visible after reaction. SEM observations support this lack of reactivity as both iron (not shown) and clay particles (Figures 3g,h) appear unaltered after 45 days.

Quantification of the extent of smectite destabilization

A quantitative estimate of the relative proportion of smectite destabilized after reaction was obtained from XRD results using the internal standard method (Hillier, 2000). Results of this quantification are presented in Table 1. The absolute precision on the relative proportion of smectite destabilized was estimated to be ±10%. This estimate corresponds to the standard deviation of twelve measurements obtained for 45 day experiments performed with sample SWy-2.

Using this quantitative XRD method it was possible to demonstrate the reactivity contrast as a function of the nature of initial smectite samples. For the different smectites presented in Figure 1, the relative proportion of destabilized smectite scatters indeed from 0-95%. Trioctahedral smectites (SapCa-2 and SapFe08 samples) were essentially unaffected as a result of their interactions with iron, while the dioctahedral smectites were systematically destabilized. Montmorillonite (20 and 50% of destabilized smectite for SAz-1 sample and

267 SWy-2 samples, respectively) and beidellites (40, 60 and 70% of destabilized smectite for
268 CP4, SbId, and Drayton samples, respectively) were less destabilized than ferruginous
269 smectites or nontronites (90 and 95% of destabilized smectite for SWa-1 and Garfield
270 samples, respectively).

271 These quantification results were positively correlated to the estimates made using
272 CEC measurements (Figure 4a). The precision of the CEC determination (±10%), which
273 corresponds to the standard deviation of six measurements obtained for 45 day experiments
274 performed with sample SWy-2, is similar to that of the XRD method. A good correlation was
275 also obtained with the IR quantification results except for the Drayton sample (Figure 4b)
276 which contains a significant proportion of ferric iron (0.47 per $O_{10}(OH)_2$ – Table 1). Precision
277 was estimated from the standard deviation of six measurements obtained for 45 day
278 experiments performed with sample SWy-2. IR measurements of reaction progress were
279 found to be less precise (±15%) than those using XRD and CEC methods mostly as a result of
280 the uncertainty on the baseline determination. In addition, note that IR results obtained on raw
281 materials may be correlated with XRD data only in the absence of kaolinite which exhibits a
282 band at 911 cm^{-1} which may interfere with the Al-Al-OH, Al-Fe-OH and Al-Mg-OH vibration
283 modes.

284 For the three quantification methods, the possible influence of the newly-formed clay
285 phases was neglected. This approximation was justified by the nature (crondstedtite, odinite)
286 of the newly-formed phases (Lantenois, 2003; Lantenois *et al.*, 2005). These 1:1
287 phyllosilicates were indeed non-swelling species thus exhibiting an extremely low CEC. In
288 addition, these phases include a large amount of structural iron. As a result, the (02,11) band
289 of these iron-rich 1:1 phyllosilicates was significantly shifted towards lower angles (at
290 ~4.7 Å) as compared to the (02,11) band of initial smectite samples (at 4.45-4.56 Å for the
291 whole compositional range). In addition the intensity of the (02,11) band of these iron-rich 1:1

phyllosilicates was found to be extremely low, thus not affecting significantly the XRD measurements (Lantenois, 2003; Lantenois *et al.*, 2005). The OH bending bands observed for these iron-rich 1:1 phyllosilicates were also shifted towards lower frequencies (750-800 cm^{-1} – Lantenois, 2003; Lantenois *et al.*, 2005) as compared to initial Al-rich smectites (820-940 cm^{-1}).

Kinetics of smectite destabilization

XRD quantification of the relative proportion of smectite destabilized after reaction also allowed deriving the kinetics of this destabilization reaction. For example, XRD patterns obtained for samples SbId reacted for 0, 5, 15, 30 and 45 days are presented in Figure 5. These experimental patterns are normalized to the (012) reflection of corundum so that the relative intensity of the (02,11) band can be compared for all samples. The relative proportion of smectite destabilized was estimated from the intensity decrease of this (02,11) band as a function of reaction time (0-120 days). Results are plotted in Figure 6 for four samples (SbId, Garfield, SWy-2 and SapCa-2). As described qualitatively, no reaction was observed for sample SapCa-2. For dioctahedral smectites, the relative proportion of destabilized smectite increases with time to reach a steady-state plateau after 30-45 days. The amount of destabilized smectite obtained after 45 days can be considered as the final one for all smectites. As was qualitatively observed the extent of smectite destabilization varies significantly as a function of the initial samples (50%, 60% and 95% of destabilized smectite for the SWy-2, SbId and Garfield samples, respectively)

315 # DISCUSSION

316

317 Quantification by XRD of the relative proportion of destabilized smectite allowed
318 demonstrating that reaction progress strongly depends on the nature of the initial smectite
319 sample, and that reaction kinetics cannot account for the reactivity contrast between different
320 smectite samples. In the following discussion, the origin of these contrasting reactivities will
321 be sought, and the influence of some structural characteristics of smectites will be discussed
322 to hypothesize reaction mechanisms for the destabilization of smectite.

323

324 ## *Influence of pH on smectite destabilization*

325

326 The initial solution pH, which is obtained by equilibrating the different smectite
327 samples in water, depends on the nature of the smectite, and varies from 7.5-10.5 (SbId-1 and
328 SWy-2, respectively – Table 2). To assess the impact of this parameter on reaction progress,
329 the relative proportion of destabilized smectite was determined as a function of the initial pH
330 for sample SWy-2. Initial pH was adjusted by adding HCl or NaOH to the initial mixture.
331 Relative proportion of destabilized smectite is reported in Table 3. When initial pH is basic
332 (8-12 pH range), the nature of the reaction products and the reaction progress are independent
333 on pH (Table 3). Conversely, reaction is dramatically different when initial pH is mildly
334 acidic to neutral. In such case, a large proportion of metal iron is dissolved, whereas iron
335 oxides, identified as magnetite using XRD (data not shown), precipitate extensively. In
336 addition, smectite appears unaffected (Table 3). A similar reaction, with the precipitation of
337 magnetite and the stability of smectite, was observed for SapCa-2 and Garfield samples when
338 initial pH was mildly acidic to neutral (Table 3).

Under mildly acidic to neutral pH conditions such as those of the present study (pH = 6), smectite remains unaltered in presence of metal iron whatever its nature. However, smectite plays a catalytic role as in the same experimental conditions (45 days, 80°C , initial pH = 6) metal iron is not destabilized in the absence of smectite whereas in presence of smectite metal iron is oxidized, most likely from its interaction with solution protons, to form magnetite according to the following reaction:

$$Fe^{\circ} + 2H^{+} \rightarrow Fe^{2+} + H_2 \ (\times 3)$$

$$2Fe^{2+} + 2H^{+} \rightarrow 2\ Fe^{3+} + H_2$$

$$Fe^{2+} + 2\ Fe^{3+} + 4\ H_2O \rightarrow Fe_3O_4 + 8\ H^{+}$$

$$3\ Fe^{\circ} + 4\ H_2O \rightarrow Fe_3O_4 + 4\ H_2 \qquad (3)$$

In our experiments, the production of gaseous H_2 during the reaction was not observed as Nalgene® reactors were H_2 porous.

Under more basic pH conditions (pH > 7 obtained from the addition of NaOH if necessary), the reaction is dramatically different as dioctahedral smectites are involved in the reaction. Dioctahedral smectites are then destabilized to form new clay phases according to the following reaction:

$$\text{Metal iron} + \text{smectite} \rightarrow \text{1:1 iron-rich phyllosilicate} + \text{iron oxides} \qquad (4)$$

Under these basic pH conditions, destabilization of dioctahedral smectite is systematic but the amount of destabilized smectite varies significantly from one sample to the other most likely as a function of the initial smectite crystal chemistry. Note that except for K-saturated smectites the equilibration pH of smectite with water is basic. The pH is essentially unaffected by iron-clay interactions.

Influence of smectite crystal chemistry on smectite destabilization

Influence of the di- or tri-octahedral character. Although initial pH values are alike, and basic, for both di- and tri-octahedral smectites, the reactivity of trioctahedral smectites is strikingly different from that of dioctahedral ones. Dioctahedral smectites are indeed systematically destabilized as the result of their interaction with metal iron whereas trioctahedral smectites remain unaffected under similar experimental conditions (Figures 1, 6). This lack of reactivity is independent on the iron content of trioctahedral smectites and on the nature of the interlayer cation.

Influence of structural Fe^{3+}. As can be seen in Figure 6 and in Table 1, nontronite and ferruginous smectites are thoroughly destabilized as the result of their interaction with metal iron. In both cases, Fe^{3+} is the predominant cation in the octahedral sheet of these 2:1 expandable phyllosilicates which exhibit mostly tetrahedral substitutions (Table 1). By contrast, the extent of the destabilization is much reduced for smectites that are not iron-rich, whatever the origin of the layer charge deficit. However, this decrease of reactivity is less important for beidellites (tetrahedral layer charge) than for montmorillonites (octahedral layer charge) for a given Fe^{3+} content. To illustrate further the influence of the amount of structural iron on smectite destabilization, XRD patterns of reacted and unreacted samples are compared in Figures 1 and 7 for dioctahedral smectites with predominant tetrahedral charges (beidellites). Their octahedral Fe^{3+} content which ranges from 0.0-1.9 per $O_{10}(OH)_2$. Relative proportions of destabilized smectites are reported as a function of the Fe^{3+} content in Figure 8. No reaction is observed when no structural Fe^{3+} is present in dioctahedral smectites, and smectite is not destabilized (Figures 7a, 8). The presence of structural Fe^{3+} is thus an essential condition for the destabilization of dioctahedral smectites when in contact with metal iron. The minimum amount of structural Fe^{3+} necessary to induce this destabilization is extremely

low as 60% of samples SbId is destabilized after 45 days of reaction with metal iron, in spite of its limited Fe^{3+} content (0.1 atom per $O_{10}(OH)_2$). In addition to this essential triggering role, the reactivity of dioctahedral smectite is clearly enhanced by an increased content of octahedral Fe^{3+} (Figure 8). However, this parameter is not the only structural parameter influencing smectite reactivity as, for example, the relative proportion of destabilized smectite is much higher for sample SbId than for sample CP4, in spite of the higher Fe^{3+} content in the latter sample (Figures 1c,d, 8 – Table 1).

Influence of the interlayer cation composition. The cation composition of smectite interlayers appears as an additional parameter influencing the reactivity of dioctahedral smectites. All samples used in the experiments reported to this point were unprocessed, and Ca^{2+} was usually predominant in their interlayer spaces (Table 1). However, K^+ was also present in CP4 and SbId, whereas Na^+ was present in several samples (SbId, SWy-2, SAz-1), and Mg^{2+} in Drayton sample. To assess the influence of the interlayer cation composition on smectite reactivity, three smectite samples (SWy-2, SAz-1 and Garfield) were reacted with metal iron following their saturation with Na^+, Ca^{2+}, and K^+. XRD patterns of reacted SWy-2 samples are presented in Figure 9, whereas the relative proportions of smectite destabilized after 45 days of reaction with metal iron are reported in Table 4. If Ca-saturated smectites are used as a reference, smectite destabilization is enhanced for Na-saturated smectites whereas it is decreased for K-saturated samples.

The reactivity contrast observed as a function of the interlayer cation composition is most likely related to the hydration of smectite which varies as a function of the interlayer cation (Norrish, 1954; Pons *et al.*, 1981). The $d_{(001)}$ basal spacing of K^+-saturated smectites varies indeed from 12.5-15.5 Å in aqueous solution (Mamy, 1968; Besson and Tchoubar, 1980), whereas that of Ca^{2+}-saturated smectites is 18.6-19.2 Å (Suquet, 1978). The $d_{(001)}$ basal spacing of Na^+-saturated smectites is not limited (osmotic swelling – Suquet *et al.*, 1981). No

significant collapse of smectite interlayers is expected as the ionic strength of the solutions, and more specifically the concentration of alkali and alkali-earth cations, remains low after reaction (Table 2). The enhanced reactivity observed for the most hydrated samples ($Na^+ > Ca^{2+} > K^+$) indicates that the ability of solution cations to access smectite interlayers is a key parameter to smectite destabilization.

Accordingly, the interlayer cation composition of samples CP4 ad SbId is likely responsible for their contrasting reactivity which does not seem to be consistent with their respective Fe^{3+} contents (Figure 8, Table 1). Specifically, the presence of Na^+ in the interlayers of sample SbId most likely enhances its reactivity as compared to sample CP4 in spite of the higher iron content in the latter sample. The influence of the cation interlayer composition may also account for the different reactivity exhibited by populations of particles observed in sample CP4. Using TEM-EDX, two populations of particles were indeed differentiated from their morphology, as "rolled" and "flat" particles were identified in this sample (Figure 10). The chemical analysis of these two types of particles revealed that although the composition of the 2:1 layers was identical in both cases, the two populations differed by their interlayer cation composition as the following structural formulae were derived for "rolled" and "flat" particles, respectively (average values from twelve analyses):

$$(Ca_{0.18}\ K_{0.03})[Fe^{(III)}_{0.28}Al_{1.72}][Si_{3.60}Al_{0.40}]\ O_{10}(OH)_2 \quad (5)$$

$$(Ca_{0.13}\ K_{0.13})[Fe^{(III)}_{0.31}Al_{1.69}][Si_{3.60}Al_{0.40}]\ O_{10}(OH)_2 \quad (6)$$

After reaction with metal iron, no remnant "rolled" particles were observed and only "flat" particles persisted. This is likely due to the increased proportion of K^+ in the interlayer of the latter particles which reduces their reactivity. Note that because long-term experiments were not performed on homoionic samples, it is not clear if the relative proportion of smectite ultimately destabilized varies from one cation to the other, or if the nature of the interlayer cation essentially influences the destabilization rate.

437

438 *Towards a possible model for smectite destabilization*

439

440 *Experimental constrains.* From the above observations, several structural features appear as
441 essential to the destabilization of smectite when in contact with metal iron. First, the smectite
442 should be dioctahedral and should contain octahedral Fe^{3+}. In addition, the accessibility of its
443 interlayer space is a key parameter for the apparent reactivity of the dioctahedral smectite.
444 Finally, when comparing experiments run at different pH values, structural protons of the
445 smectite are likely involved in the oxidation of metal iron under neutral-to-alkaline
446 conditions. In mildly acidic to neutral conditions, solution protons are abundant enough so
447 that smectite is used essentially as a catalyst but is not directly involved in the corrosion of
448 iron following Reaction (3). Under high pH conditions, protons are essentially present as OH
449 groups in smectite, as both smectite interlayer and edge sites are essentially deprotonated
450 under such pH conditions.

451 Deprotonation of these hydroxyl groups may occur under a variety of physico-
452 chemical conditions for dioctahedral smectites (Russel, 1979; Jaymes and Bigham, 1987;
453 Heller-Kallai and Rozenson, 1981; Heller-Kallai, 2001 – Figure 11a). In particular, the
454 presence of inorganic proton acceptors, usually alkali halides or alkali hydroxides, has been
455 reported to induce such a deprotonation reaction (Heller-Kallai, 1975a, 1975b, 2001; Russel,
456 1979; Heller-Kallai and Rozenson, 1981; Heller-Kallai and Mosser, 1995). In our case, metal
457 iron is likely the proton acceptor triggering smectite deprotonation. Metal iron is oxidized in
458 turn as the result of its interaction with protons (Figure 11b) according to Reaction (3). The
459 high affinity of metal iron for smectite and their resulting interactions have for example been
460 recognized as causing the oxidation of steel pipes when using clay-containing drilling fluids
461 (Tomoe *et al.*, 1999; Cosultchi *et al.*, 2003). According to this model, both the oxidation of

462 metal iron and the deprotonation of smectite are strongly favored by the accessibility of metal
463 iron to smectite interlayer. With this respect the osmotic swelling commonly observed for Na-
464 saturated smectites significantly enhances the accessibility of metal iron particles to smectite
465 interlayers, thus favoring the deprotonation reaction. In turn, deprotonation increases
466 considerably the layer charge deficit in smectite octahedral sheet and thus enhances their
467 reactivity.

468 Deprotonation thus appears as the driving force for the oxidation of metal ion, and for
469 the initiation of smectite destabilization. Accordingly, the presence of Fe^{3+} in the octahedral
470 sheet of smectite appears as an essential parameter for these two reactions as $MeFe^{3+}OH$
471 groups are known to deprotonate preferentially in dioctahedral smectites (Heller-Kallai,
472 1975a, 2001; Russel, 1979; Jaymes and Bigham, 1987). It is not clear however if
473 deprotonation of Fe^{3+}-free dioctahedral smectites is not occurring, or is extremely limited, or
474 if deprotonation is not the limiting step for the destabilization of Fe^{3+}-free dioctahedral
475 smectites. However, although Heller-Kallai (1975a) showed that deprotonation occurs even in
476 Fe^{3+}-free dioctahedral smectite, we have not observed iron corrosion resulting from this
477 process in the SbS-1 experiments.

478 *Destabilization of smectite.* Following its initial deprotonation, destabilization of smectite is
479 probably favored by the presence of Fe^{2+} in solution as a result of the oxidation of metal iron.
480 Specifically, the high affinity of Fe^{2+} for smectite edge surface sites (Tournassat *et al.*, 2005 –
481 Figure 11c) is likely a key factor for the subsequent destabilization of smectite. Following
482 their sorption on these edge sites, Fe^{2+} cations are readily oxidized as shown by Tournassat *et*
483 *al.* (2005), the electron acceptors being octahedral Fe^{3+} from smectite structure (Figure 11c).
484 Note that following their oxidation, sorbed Fe cations may also accept electrons either from
485 solution Fe^{2+} cations or from iron metal to restore their +II valency (Figure 11d). As a result
486 of both its initial deprotonation and of the subsequent reduction of its structural Fe^{3+}, the

charge deficit in the octahedral sheet of smectite is dramatically increased and Fe^{2+} cations likely migrate in its interlayers to compensate for the increased layer charge (Figure 11d). The inceased concentration of Fe^{2+} in solution resulting from the oxidation of the metal iron also favors a Fe^{2+}-for-Na^{+} cation exchange. Such Fe^{2+}-for-Na^{+} cation exchange has been shown to occur in reducing environments cations (Kamei *et al.*, 1999).

The effective ionic radius of Fe^{2+} cations (0.78 Å – Shannon, 1976) is smaller than the limit size approximated by Heller-Kallai (2001) at 0.85 Å allowing migration of the cations into the silicate layer. It is thus likely that interlayer Fe^{2+} cations actually migrate either into the di-trigonal cavities of smectite tetrahedral sheets or in smectite octahedral sheet (Figure 11e). This migration is similar to that of Li^{+} cations (0.76 Å – Shannon, 1976) involved in the Hofmann-Klemen test (Hofmann and Klemen, 1950; Greene-Kelly, 1955). The migration of Li^{+} from the interlayer to the di-trigonal cavity and further to the octahedral sheet of montmorillonites has been extensively documented (Hofmann and Klemen, 1950; Greene-Kelly, 1955 ; Glaeser and Fripiat, 1976; Madejova *et al.*, 1996, 2000a, 2000b, among others). Heating to 300°C for 24 hours represent optimum experimental conditions for this migration. Migration of other divalent cations with an effective ionic radius similar to that of Li^{+} cations has also been described. For example, Cu^{2+}, Ni^{2+} and Zn^{2+} cations (0.73, 0.69 and 0.74 Å, respectively) migrate from montmorillonite interlayers to the di-trigonal cavity between 100-300°C (Heller-Kallai and Mosser, 1995; Mosser *et al.*, 1997; Madejova *et al.*, 1999; Palkova *et al.*, 2003) and to the octahedral sheet at higher temperature (Brindley and Ertem, 1971; McBride and Mortland, 1974; Heller-Kallai and Mosser, 1995; Emmerich *et al.*, 1999).

These conditions are much more energetically favorable than those involved in our experiments. However, partial migration of Li at least to the di-trigonal cavity has been reported for Li-saturated montmorillonite heated to 105°C for 24 hours (Madejova *et al.*, 1996). In our experiments, three factors compensate for the low thermal energy available. The

512 first one is the extremely strong layer charge deficit which, according to the structural model
513 proposed for smectite destabilization occurring in our experiments, arises both from the
514 deprotonation of hydroxyl groups and from the reduction of structural Fe^{3+}. Note that the need
515 for an octahedral layer charge deficit is the fundamental basis for the migration of Li^{+} cations
516 involved in the Hofmann-Klemen test (Hofmann and Klemen, 1950). Furthermore, the
517 positive influence of an increased layer charge deficit on the migration of divalent cations has
518 been reported by Heller-Kallai and Mosser (1995, e.g.). These authors observed indeed an
519 increased amount of Cu in samples that were deprotonated first. As described by Heller-Kallai
520 and Mosser (1995), the positive effect of the initial deprotonation is not restricted to the
521 increased layer charge deficit and the second factor favoring the migration of Fe^{2+} cations is
522 the absence of protons inside the di-trigonal cavity. As a consequence, there is no electrostatic
523 repulsion to the migration of Fe^{2+} cations into the octahedral sheet. Reaction time represents
524 the third factor compensating for the low thermal energy in our experiments. Our experiments
525 lasted indeed for 45 days whereas the common duration of experiments leading to the
526 formation of reduced-charge smectites is 24 hours. Initial migration of Fe^{2+} cations to the di-
527 trigonal cavity is likely favored by an increased undersaturation of the oxygen atoms present
528 at the surface of the 2:1 layers, that is by the existence of layer charge deficit in smectite
529 tetrahedral sheets. Such location of layer charge deficit favors indeed the initial partial
530 dehydration of interlayer Fe^{2+} cations, allowing for the formation of an inner-sphere complex
531 necessary for their migration, and thus accounts for the increased reactivity of beidellite
532 samples as compared to montmorillonite ones for a given iron content (see for example SAz-1
533 and SbId samples – Table 1). The formation of such inner-sphere complexes has been widely
534 documented in hydrated beidellites for monovalent interlayer cations, both from XRD (Ben
535 Brahim *et al.*, 1983a, 1983b, 1984), and infrared (Pelletier *et al.*, 2003) studies, and from
536 Monte-Carlo modeling (Chang *et al.*, 1995; Skipper *et al.*, 1995).

In our experiments, migration of Fe^{2+} cations in the octahedral sheet of smectite does not induce a collapse of smectite interlayers as these new octahedral Fe^{2+} compensate essentially for the layer charge deficit resulting from the deprotonation of hydroxyl groups and from the reduction of structural Fe^{3+}, but not for the initial charge deficit of the 2:1 layers. The presence of hydrated interlayer cations, part of which are Fe^{2+}, still compensates for this initial charge deficit, and keeps the smectite interlayers expanded. The migration of Fe^{2+} cations in the octahedral sheet of smectite is rather thought to be responsible for the destabilization of smectites induced by their interaction with metal iron. Destabilization is indeed thought to result from the presence of trioctahedral domains in the octahedral sheet of reacted smectite (Figure 11e). The coexistence of both dioctahedral and trioctahedral domains is widely reported in natural 1:1 phyllosilicates but is limited in 2:1 phyllosilicates (Bailey, 1980). The existence of 2:1 phyllosilicates with a mixed di- and tri-octahedral occupancy is indeed essentially limited to mica species exhibiting a tetrahedral charge (muscovite-zinnwaldite or muscovite-phlogopite series – Monier and Robert, 1986). In such species the increased dimensions of the octahedral sheet in the **ab** plane is accommodated by the reduction of the tetrahedral tilt angle. In smectites, and more especially in montmorillonites, the amount of tetrahedral substitutions is limited and the tetrahedral tilt angle is thus minimum. As a consequence, such 2:1 phyllosilicates are unable to accommodate the presence of trioctahedral domains containing large cations and are thus destabilized by the migration of Fe^{2+} cations in their octahedral sheet.

According to the conceptual model hypothesized for smectite destabilization, the lack of reactivity of trioctahedral smectites results from three main factors. The first two are related to the absence of Fe^{3+} cations in the octahedral sheet of these smectite samples. The first effect of this absence is to make deprotonation of hydroxyl groups more difficult as, in dioctahedral smectites, $MeFe^{3+}OH$ groups are known to deprotonate preferentially (Heller-

562 Kallai, 1975a, 2001; Russel, 1979; Jaymes and Bigham, 1987). The second effect is the
563 absence of cations that may be reduced in the octahedral sheet of trioctahedral smectites. The
564 combination of these two effects prevents building a strong layer charge deficit in the
565 octahedral sheet of trioctahedral smectites. The third factor leading to the lack of reactivity of
566 trioctahedral smectite is the obvious impossibility for cations to migrate in this octahedral
567 sheet which is fully occupied.
568 *Influence of structural Fe on smectite destabilization*. In the above conceptual model for
569 smectite destabilization, the effect of an increased proportion of structural iron on smectite
570 destabilization is dual. The first effect arises from the increased proportion of $MeFe^{3+}OH$
571 groups that will readily deprotonate when in contact with metal iron. The larger number of
572 deprotonated hydroxyl groups requires in turn the presence of a larger number of Fe^{2+} cations
573 in smectite interlayers to balance the charge. The second effect is directly related to the
574 increased proportion of structural Fe^{3+} in smectite octahedral sheet. This allows for a larger
575 proportion of smectite octahedral sheets to present dramatic charge deficit leading to the
576 migration of interlayer Fe^{2+} in the 2:1 layer, thus destabilizing it. On the other hand, the
577 presence of Fe^{3+} in smectite tetrahedral sheet does not enhance smectite reactivity as these
578 cations cannot be reduced because of steric constrains arising from their tetrahedral
579 environment.
580
581 ## CONCLUSION
582
583 The present study aimed at assessing the stability of smectites, which represent the
584 reactive components of engineered and geological barriers, when in contact with metal iron at
585 temperatures realistic in the context of nuclear waste disposal (80°C). Dioctahedral smectites
586 are thoroughly destabilized under such conditions, leading to the precipitation of magnetite

587 and of 1:1 iron-rich phyllosilicates [odinite, crondstedtite – Lantenois (2003), Lantenois *et al.*
588 (2005)]. Smectite destabilization is systematic for neutral-to-basic pH conditions (pH > 7),
589 whereas in mildly acidic to neutral pH conditions, a significant proportion of metal iron is
590 corroded to form magnetite without smectite destabilization.

591 An XRD method was developed to quantify the extent of smectite destabilization. This
592 method was validated against CEC measurements and IR spectroscopy results. Structural and
593 crystal-chemical factors favoring smectite destabilization were thus determined. These
594 parameters include the amount of octahedral iron, the presence of tetrahedral substitutions,
595 and the nature of interlayer cations, and a conceptual model was hypothesized to account for
596 smectite destabilization. According to this model, the formation of trioctahedral clusters
597 resulting from the migration of Fe^{2+} cations into the octahedral sheet of the 2:1 layer is
598 responsible for smectite destabilization as tetrahedral sheets are unable to accommodate the
599 larger dimensions of these domains.

600 In agreement with experimental results, the dioctahedral character of the initial
601 smectite is an essential condition for its destabilization in the proposed model. As a result the
602 non-reactivity of trioctahedral smectites appears as an important point for the conception of
603 engineered barriers for nuclear waste disposal, although natural deposits of trioctahedral
604 smectite are uncommon.

605

606 ## ACKNOWLEDGMENTS

607

608 J.-L. Robert is thanked for the insightful discussions which allowed improving the
609 present manuscript. The precious help of R. Champallier and J.-L. Robert, who prepared the
610 synthetic smectite samples, and of W.P. Gates, who provided us with the CP4 and Drayton
611 Fe-beidellites, is gratefully acknowledged. J.-M. Bény and P. Benoist (I.S.T. Orléans) are

612 thanked for their assistance during infrared spectroscopy and CEC measurements,
613 respectively. The present manuscript was improved by the constructive reviews of Lisa
614 Heller-Kallaï, Will P. Gates and AE Peter Komadel.

615

616 **REFERENCES**

617

618 Aogaki, R. (1999) Non-equilibrium fluctuations in the corrosion. pp 217-305 in: Modern
619 aspects of electrochemistry (R.E White, B.E. Conway and J.O'M. Bockris editors).
620 Kluwer, New York.

621 Bailey, S.W. (1980) Structures of layer silicates. pp. 1-123 in Crystal Structures of Clay
622 Minerals and their X-ray Identification (G.W. Brindley and G. Brown editors).
623 Mineralogical Society, London.

624 Ben Brahim, J., Armagan, G., Besson, G. and Tchoubar, C. (1983a) X-ray diffraction studies
625 on the arrangement of water molecules in a smectite. I. Homogeneous two-water-layer
626 Na-beidellite. *Journal of Applied Crystallography*, **16**, 264-269.

627 Ben Brahim, J., Besson, G. and Tchoubar, C. (1983b) Layer succession and water molecules
628 arrangement in a homogeneous two-water layer Na-smectite. Pp. 65-75 in:
629 *Proceedings of the 5th Meeting of the European Clay Groups*, Prague.

630 Ben Brahim, J., Besson, G. and Tchoubar, C. (1984) Etude des profils des bandes de
631 diffraction X d'une beidellite-Na hydratée à deux couches d'eau. détermination du
632 mode d'empilement des feuillets et des sites occupés par l'eau. *Journal of Applied*
633 *Crystallography*, **17**, 179-188.

634 Besson, G. and Tchoubar, C. (1980) Exemple d'ordre-désordre par rotation des feuillets dans
635 la montmorillonite potassique. *Bulletin de Minéralogie,* **103**, 429-433.

636 Brindley, G.W. and Ertem G. (1971) Preparation and solvation properties of some variable
637 charge montmorillonites. *Clays and Clay Minerals*, **19**, 399-404.
638 Chang, F.R.C., Skipper, N.T. and Sposito, G. (1995) Computer simulation of interlayer
639 molecular structure in sodium montmorillonite hydrates. *Langmuir*, **11**, 2734-2741.
640 Cosultchi, A., Rossbach, P. and Hernandez-Calderon, I. (2003) XPS analysis of petroleum
641 well tubing adherence. *Surface and Interface Analysis*, **35**, 239-245.
642 Cuadros, J. and Altaner, S.P. (1998) Compositional and structural features of the octahedral
643 sheet in mixed-layer illite/smectite from bentonites. *European Journal of Mineralogy*,
644 **10**, 111-124.
645 Emmerich, K., Madsen, F. T. and Kahr G. (1999) Dehydroxylation behavior of heat-treated
646 and steam-treated homoionic *cis*-vacant montmorillonites. *Clays and Clay Minerals*,
647 **47**, 591-604.
648 Farmer, V.C. (1974) The IR Spectra of minerals. 539 p. Mineralogical Society, London.
649 Gaboriau, H. (1991) Interstratifiés smectite-kaolinite de l'Eure. Thesis, Université d'Orléans,
650 274p.
651 Gates, W.P., Slades, P.G., Manceau, A. and Lanson, B. (2002) Site occupancies by iron in
652 nontronites. *Clays and Clay Minerals*, **50**, 223-239.
653 Glaeser R. and Fripiat J. J. (1976) Hydratation des smectites et démixtion des cations Li, Na
654 en fonction de la localisation des substitutions isomorphiques. *Clay Minerals*, **11**, 93-
655 99.
656 Goodman, B.A., Russell, J.D., Fraser, A.R. and Woodhams, F.W.D. (1976) A mössbauer and
657 I.R. spectroscopic study of the structure of nontronite. *Clays and Clay Minerals*, **24**,
658 53-59.
659 Greene-Kelly, L. (1955) Dehydration of montmorillonite minerals. *Mineralogical Magazine*,
660 **30**, 604-615.

661 Guillaume, D., Neaman, A., Cathelineau, M., Mosser-Ruck, R., Peiffert, C., Abdelmoula, M.,
662 Dubessy, J., Villieras, F., Baronnet, A. and Michau, N. (2003) Experimental synthesis
663 of chlorite from smectite at 300°C in the presence of metallic Fe. *Clay Minerals*, **38**,
664 281-302.
665 Habert, B. (2000) Réactivité du fer dans les gels et les smectites. Thesis, Université Paris 6,
666 Paris, 227p.
667 Hamilton, D.L. and Henderson, C.M.B. (1968) The preparation of silicate compositions by a
668 gelling method. *Mineralogical Magazine*, **36**, 832-838.
669 Heller-Kallai, L. (1975a) Interaction of montmorillonite with alkali halides. S. W. Bailey (ed.)
670 proceding of international clay conference, Mexico, p. 361-375.
671 Heller-Kallai, L. (1975b) Montmorillonite-alkali halide interaction : a possible mechanism of
672 illitization. *Clays and Clay Mineral*, **23**, 462-467.
673 Heller-Kallai, L. (2001) Protonation-deprotonation of dioctahedral smectites. *Applied Clay*
674 *Science*, **20**, 27-38.
675 Heller-Kallai, L. and Rozenson, I. (1981) Nontronite after acid or alkali attack. *Chemical*
676 *Geology*, **32**, 95-102.
677 Heller-Kallai, L. and Mosser, C. (1995) Migration of Cu ions in Cu montmorillonite heated
678 with and without alkali halides. *Clays and Clay Minerals*, **43**, 738-743.
679 Hillier, S. (2000) Accurate quantitative analysis of clay and other minerals in sandstones by
680 XRD: comparison of a Rietveld and a reference intensity ratio (RIR) method and the
681 importance of sample preparation. *Clay Minerals*, **35**, 291-302.
682 Hofmann, V. and Klemen, R. (1950) Verlust der Austauschfähigkeit von lithiumionen aus
683 Bentonit durch Erhitzung. *Zeitschrift für Anorganische und Allgemeine Chemie*, **262**,
684 95-99.

685 Jaymes, W. F. and Bigham, J. M. (1987) Charge reduction , octahedral charge, and lithium
686 retention in heated, Li-saturated smectites. *Clays and Clay Minerals*, **35**, 440-448.
687 Kamei, G., Oda, C., Mitsui, S., Shibata, M., Shinozaki, T. (1999) Fe(II)-Na ion exchange at
688 interlayers of smectite : adsorption-desorption experiments and a natural analogue.
689 *Engineering Geology*, **54**, 15-20.
690 Kloprogge, J.T., Komarnene, S. and Amonette, J.E. (1999) Synthesis of smectite clay
691 minerals: a critical review. *Clays and Clay Minerals*, **47**, 529-554.
692 Kohler, E. (2001) Réactivité des mélanges synthétiques smectite/kaolinite et
693 smectite/aluminium gel en présence d'un excès de fer métal. DRT, Université d'Evry
694 val d'Essonne, Evry, 101p.
695 Lantenois, S. (2003). Réactivité fer métal/smectites en milieu hydraté à 80°C. Ph.D. thesis,
696 Université d'Orléans, Orléans, 188p
697 Lantenois, S., Lanson, B., van Aken, P. A., Jullien, M., Muller, F. and Plancon A. (2005)
698 Experimental study of metal iron - smectites interactions at low temperature :
699 characterisation of the newly-formed phases. Geochimica Et Cosmochimica Acta (in
700 preparation).
701 Madejova, J. and Komadel, P. (2001) Baseline studies of the clay minerals society source
702 clays: infrared methods. *Clays and Clay Minerals*, **49**, 410-432.
703 Madejova, J., Arvaiova, B. and Komadel, P. (1999) FTIR spectroscopic characterization of
704 thermally treated Cu^{2+}, Cd^{2+} and Li^{+} montmorillonites. *Spectrochimica Acta Part A*,
705 **55**, 2467-2476.
706 Madejova, J., Bujdak, J., Gates, W. P. and Komadel, P. (1996) Preparation and infrared
707 spectroscopic characterization of reduced-charge montmorillonite with various Li
708 contents. *Clay Minerals*, **31**, 233-241.

709 Madejova, J., Bujdak, J., Petit, S. and Komadel, P. (2000a) Effects of chemical composition
710 and temperature of heating on the infrared spectra of Li-saturated dioctahedral
711 smectites. (I) Mid-infrared region. *Clay Minerals*, **35**, 739-751.
712 Madejova, J., Bujdak, J., Petit, S. and Komadel, P. (2000b) Effects of chemical composition
713 and temperature of heating on the infrared spectra of Li-saturated dioctahedral
714 smectites. (II) Near-infrared region. *Clay Minerals*, **35**, 753-761.
715 Mamy, J. (1968) Recherches sur l'hydratation de la montmorillonite: Propriétés diélectriques
716 et structure du film d'eau. Thesis, Université de Paris 6, Paris, 142p.
717 McBride, M.B. and Mortland M.M. (1974) Copper (II) interactions with montmorillonite:
718 Evidence from physical methods. *Soil Science Society of America Proceedings*, **38**,
719 408-415.
720 Monier, G., Robert, J.-L. (1986) Evolution of the miscibility gap between muscovite and
721 biotite solid solutions with increasing lithium content : an experimental study in the
722 system K_2O-Li_2O-MgO-FeO-Al_2O_3-SiO-H_2O-HF at 600°C, 2 kbar p_{H2O} : comparison
723 with natural lithium micas. *Mineralogical Magazine*, 50, 641-651.
724 Mosser, C., Michot, L. J., Villieras, F. and Romeo, M. (1997) Migration of cations in
725 copper(II)-exchanged montmorillonite and laponite upon heating. *Clays and Clay*
726 *Minerals*, **45**, 789-802.
727 Norrish, K. (1954) The swelling of montmorillonite. *Discussions of the Faraday Society*, **18**,
728 120-134.
729 Palkova, H., Madejova, J. and Righi, D. (2003) Acid dissolution of reduced-charge Li- and
730 Ni-montmorillonites. *Clays and Clay Minerals*, **51**, 133-142.
731 Pelletier, M., Michot, L.J., Humbert, B., Barres, O., D'espinose de la Callerie, J.B. and
732 Robert, J.L. (2003) Influence of layer charge on the hydroxyl stretching of

733 trioctahedral clay minerals: A vibrational study of synthetic Na- and K-saponites.
734 *American Mineralogist*, **88**, 1801-1808.
735 Perronnet, M. (2001) Etude des interactions fer-argile en condition de stockage géologique
736 profond des déchets nucléaires HAVL. DEA, ENS Géologie, Nancy, 33p.
737 Perronnet, M. (2004) Etude des interactions fer-argile en condition de stockage géologique
738 profond des déchets nucléaires HAVL. Ph.D. thesis, ENS Géologie, Nancy, 233p.
739 Pons, C.H., Rousseaux, F. and Tchoubar, D. (1981) Utilisation du rayonnement synchrotron
740 en diffusion aux petits angles pour l'étude du gonflement des smectites: I Etude du
741 système eau-montmorillonite-Na en fonction de la température. *Clay Minerals*, **16**, 23-
742 42.
743 Roux, J. and Volfinger, M. (1996) Mesures précises à l'aide d'un détecteur courbe. *Journal de*
744 *Physique*, **IV**, 127-134.
745 Russell, J.D. (1979) An infrared spectroscopic study of the interaction of nontronite and
746 ferruginous montmorillonites with alkali metal hydroxides. *Clay Minerals*, **14**, 127-
747 137.
748 Russell, J. and Fraser, A. (1994) Infrared methods in Clay mineralogy: spectroscopic and
749 chemical determinative methods. M.J. Wilson, Ed. Chapman and Hall, London, p. 11-
750 67.
751 Shannon, R. D. (1976) Revised effective ionic radii and systematic studies of interatomic
752 distances in halides and chalcogenides. *Acta Crystallographica A*, **32**, 751-767.
753 Skipper, N.T., Chang, F.R.C. and Sposito, G. (1995) Monte Carlo simulation of interlayer
754 molecular structure in swelling clay minerals. 1. Methodology. *Clays & Clay*
755 *Minerals*, **43**, 285-293.
756 Suquet, H.B. (1978) Propriétés de gonflement et structure de la saponite. Comparaison avec la
757 vermiculite. Thesis, Université Pierre et Marie Curie, Paris, 175p.

758 Suquet, H., IIyama, J.T., Kodama, H. and Pezerat, H. (1977) Synthesis and swelling
759 properties of saponites with increasing layer charge. *Clays and Clay Minerals*, **25**,
760 231-242.
761 Suquet, H., Malard, C., Copin, E. and Pezerat, H. (1981) Variation du paramètre b et de la
762 distance basale d_{001} dans une série de saponites à charge croissante: I Etats hydratés.
763 *Clay Minerals*, **16**, 53-67.
764 Tomoe, Y., Shimizu, M. and Nagae, Y. (1999) Unusual corrosion of a drill pipe in newly
765 developed drilling mud during deep drilling. *Corrosion*, **55**, 706-713.
766 Tournassat C., Charlet L. & Greneche J.-M. Interactions of Fe^{2+}, Zn^{2+}, and H_4SiO_4 at
767 clay/water interfaces: Distinguishing sorption, coadsorption, and surface oxidation
768 phenomena. Geochimica and Cosmochimica Acta, submitted
769 Vantelon, D., Pelletier, M., Michot, L.J., Barres, O. and Thomas, F. (2001) Fe, Mg and Al
770 distribution in the octahedral sheet of montmorillonites. An infrared study in the OH-
771 bending region. *Clay Minerals*, **36**, 369-379.
772

773 FIGURE CAPTIONS

774

775 **Figure 1.** XRD patterns obtained on unreacted and reacted smectite samples (upper and lower
776 patterns, respectively). Montmorillonite, beidellite, nontronite and saponite samples were
777 reacted for 45 days with metal iron at 80°C (see text for details) (a) Sample SWy-2 ,(b)
778 Sample SAz-1, (c) Sample SbId, (d) Sample CP4, (e) Sample Garfield, (f) Sample SapCa-2,
779 and (g) Sample SapFe08. Scale factor (x3) over the 20-35°2θ CoKα range. Patterns were
780 normalized by pairs to the integrated intensity of corundum (012) reflection (solid line, S).
781 The (001) reflection and the (02,11) band of the clay samples are labeled. Q indicates the
782 presence of quartz impurities in some samples (dashed lines). Dotted lines indicate the
783 reflections of newly-formed phases. These phases are labeled M, L, and P for magnetite
784 (Fe_3O_4), lepidocrocite (γ-FeOOH), and a newly formed 1:1 phyllosilicate, respectively.

785 **Figure 2**. Method for quantifying the relative proportion of destabilized smectite using IR
786 spectroscopy. (a) IR spectrum of sample SWy-2 (unreacted) before subtraction of the
787 baseline. Si-O indicates the Si-O vibrations in phyllosilicates whereas Al-Al-OH, Al-Fe-OH
788 and Al-Mg-OH refer to the OH bending mode of the respective hydroxyl groups. Q denotes
789 the two vibrations bands of quartz. (b) Decomposition assuming three Guassian-shaped
790 contributions of the OH bending zone after baseline subtraction (sample SWy-2 unreacted).

791 **Figure 3**. SEM micrographs of unreacted and reacted samples. Metal iron particles in
792 unreacted and reacted SWy-2 sample are shown on (a) and (b), respectively. (c) and (d)
793 Smectite particles in the reacted sample SWy-2. (e) Smectite particles in the initial sample
794 SWy-2. (f) Smectite particles in the reacted Garfield sample. (g) Smectite particles in the
795 initial sample SapCa-2. (h) Smectite particles in the reacted sample SapCa-2.

796 **Figure 4**. Relative proportion of destabilized smectite calculated by XRD and CEC methods
797 (a) and by XRD and infrared methods (b). Solid square: sample SapCa-2; solid triangle:

798 sample SAz-1; solid circle: sample SWy-2; solid diamond: Garfield sample; open diamond:
799 Drayton sample. The (1:1) line is shown as a solid line.

800 **Figure 5**. XRD patterns obtained for unreacted SbId sample (a) and for reacted SbId sample
801 (b-e). (b), (c), (d) and (e) correspond to 5, 15, 30 and 45 day experiments, respectively. Scale
802 factor (x3) over the 20-35°2θ CoKα range. Patterns were normalized as in Figure 1. Other
803 labels and patterns as in Figure 1.

804 **Figure 6**. Evolution of the relative proportion of destabilized smectite as a function of
805 reaction time. Symbols as in Figure 4. Open triangles: sample SbId.

806 **Figure 7**. XRD patterns obtained on unreacted and reacted beidellite samples (upper and
807 lower patterns, respectively). Patterns are ranked as a function of their structural Fe^{3+} content
808 (Table 1). Samples were reacted for 45 days with metal iron at 80°C without controlling the
809 initial pH. (a) Sample SbS-1, (b) Drayton sample, and (c) sample SWa-1. Scale factor (x3)
810 over the 20-35°2θ CoKα range. Patterns were normalized as in Figure 1. Other labels and
811 patterns as in Figure 1.

812 **Figure 8**. Relative proportion of destabilized smectite after reaction with metal iron as a
813 function of their content of structural Fe^{3+} (Table 1) Relative proportion of destabilized
814 smectite amounts was estimated using XRD on 45 day experiments.

815 **Figure 9**. XRD patterns recorded on sample SWy-2 reacted with metal iron after K-, Ca-, and
816 Na-saturation (b, c, and d, respectively). Unreacted Na-saturated sample corresponds to the
817 raw SWy-2 sample (a). Scale factor (x3) over the 20-35°2θ CoKα range. Patterns were
818 normalized as in Figure 1. Other labels and patterns as in Figure 1.

819 **Figure 10**. Transmission electron micrographs of smectite particles from sample CP4.
820 "rolled" and "flat" particles are labeled (1) and (2), respectively.

821 **Figure 11**. Conceptual model leading to the destabilization of dioctahedral smectites as a
822 result of their interaction with metal iron. (a) Deprotonation of $MeFe^{3+}OH$ groups. (b)

823 Oxidation of metal iron as a result of its interaction with released protons. (c) Sorption of Fe^{2+}
824 cations on the edges of smectite particles and reduction of structural Fe^{3+} cations. (d)
825 Migration of solution Fe^{2+} cations in smectite interlayers to compensate for the layer charge
826 deficit. Part of this migration results from a Fe^{2+}-for-Na^{+} exchange. With time, interlayer Fe^{2+}
827 cations migrate to the di-trigonal cavity and further to the octahedral sheet to compensate
828 locally for the charge deficit. (e) Coexistence of di- and tri-octahedral domains in the
829 octahedral sheet of smectite leads to its destabilization.
830

Table 1: Chemical composition of the initial smectite materials (structural formulae calculated per $O_{10}(OH)_2$) and relative proportion of smectite destabilized after reaction with metal iron for 45 days.

Sample	Garfield[a]	SWa-1[a]	Drayton[b]	CP4[b]	SbId[c]	SbS-1[c,d]	SWy-2[c]	SAz-1[c]	SapCa-2[c]	SapFe08[c,d]
Nature[e]	N	FS	B	B	B	B	M	M	S	S
Tetrahedral										
Si	3.51	3.70	3.69	3.60	3.71	3.66	3.95	4.00	3.58	3.62
Al	0.49	0.30	0.31	0.40	0.29	0.34	0.05	-	0.39	-
Fe^{3+}	-	-	-	-	-	-	-	-	0.03	0.38
charge	-0.49	-0.30	-0.31	-0.40	-0.29	-0.34	-0.05	-	-0.42	-0.38
Octahedral										
Al	0.11	0.55	1.11	1.70	1.80	2.00	1.56	1.37	-	-
Fe^{3+}	1.86	1.31	0.47	0.30	0.12	-	0.21	0.07	-	0.00
Mg	0.02	0.13	0.44	-	0.08	-	0.23	0.56	3.00	3.00
occupancy	1.99	1.99	2.02	2.00	2.00	2.00	2.00	2.00	3.00	3.00
charge	-0.05	-0.16	-0.38	0.00	-0.08	0.00	-0.23	-0.56	0.00	0.00
Interlayer										
Na	0.09	0.03	-	-	0.08	0.33	0.14	0.05	0.34	0.39
Ca	0.20	0.20	0.17	0.15	0.10	-	0.05	0.24	0.05	-
Mg	-	-	0.18	-	-	-	-	-	-	-
K	0.04	0.05	-	0.09	0.08	-	0.01	0.01	0.02	-
charge	0.53	0.48	0.70	0.39	0.36	0.33	0.25	0.54	0.46	0.39
Smectite destab. (wt %)	95	90	70	40	60	0	50	20	0	0

Note: [a] From Gates *et al.* (2002). Interlayer composition of raw materials was determined from electron microprobe analysis, [b] EDX analysis on a transmission electron microscope, [c] electron microprobe analysis, [d] synthetic clays. [e] N, FS, B, M, S correspond to nontronite, ferruginous smectite, beidellite, montmorillonite and saponite respectively.

Table 2: Chemical composition of the solution after reaction of smectite samples with metal iron for 45 days.

	Si	Al	Fe	Mg	Na	Ca	K	Initial pH	Final pH
SapCa-2	0.0	0.0	0.0	0.0	10.0	4.0	0.0	9.5	10.0
SapCa-2 Ref	0.0	0.0	0.0	0.0	7.0	2.0	0.0	9.5	9.5
SWy-2	6.5	0.1	0.0	0.3	115	3.5	3.0	10.0	10.5
SWy-2 Ref	0.0	0.0	0.0	0.0	11.0	0.0	0.0	10.0	10.0
SbId	2.0	0.4	0.0	0.3	17.0	28.0	14.0	7.5	7.5
SbId Ref	0.0	0.0	0.0	0.0	1.0	2.0	1.0	7.5	7.5
Garfield	0.0	0.0	0.0	0.0	17.5	22.5	1.0	8.5	9.5
Garfield Ref	0.0	0.0	0.0	0.0	10.0	1.0	2.0	8.5	9.0

Note: Concentrations are given in $mg.L^{-1}$. Initial and final pH values were measured before and after reaction, respectively. Regular sample names correspond to the reaction of a given smectite sample with metal iron for 45 days at 80°C. Ref samples correspond to the reaction of a given smectite sample for 45 days at 80°C without metal iron.

Table3: Relative proportion of smectite destabilized (weight %) as a function of the initial solution pH.

pH	SWy-2	SapCa-2	Garfield
6	0%	0%	0%
8	50%	-	95%
10	50%	0%	-
12	50%	-	-

Note: Relative proportion of destabilized smectite is estimated using the XRD method.

Table 4: Relative proportion of smectite destabilized (weight %) as a function of the cation interlayer composition.

	SAz-1	SWy-2	Garfield
K	-	0%	50%
Ca	20%*	20%	95%*
Na	40%	50%*	-

Note: Relative proportion of destabilized smectite is estimated using the XRD method. * indicate raw samples, with the corresponding predominant interlayer cation.

Figure 1 :

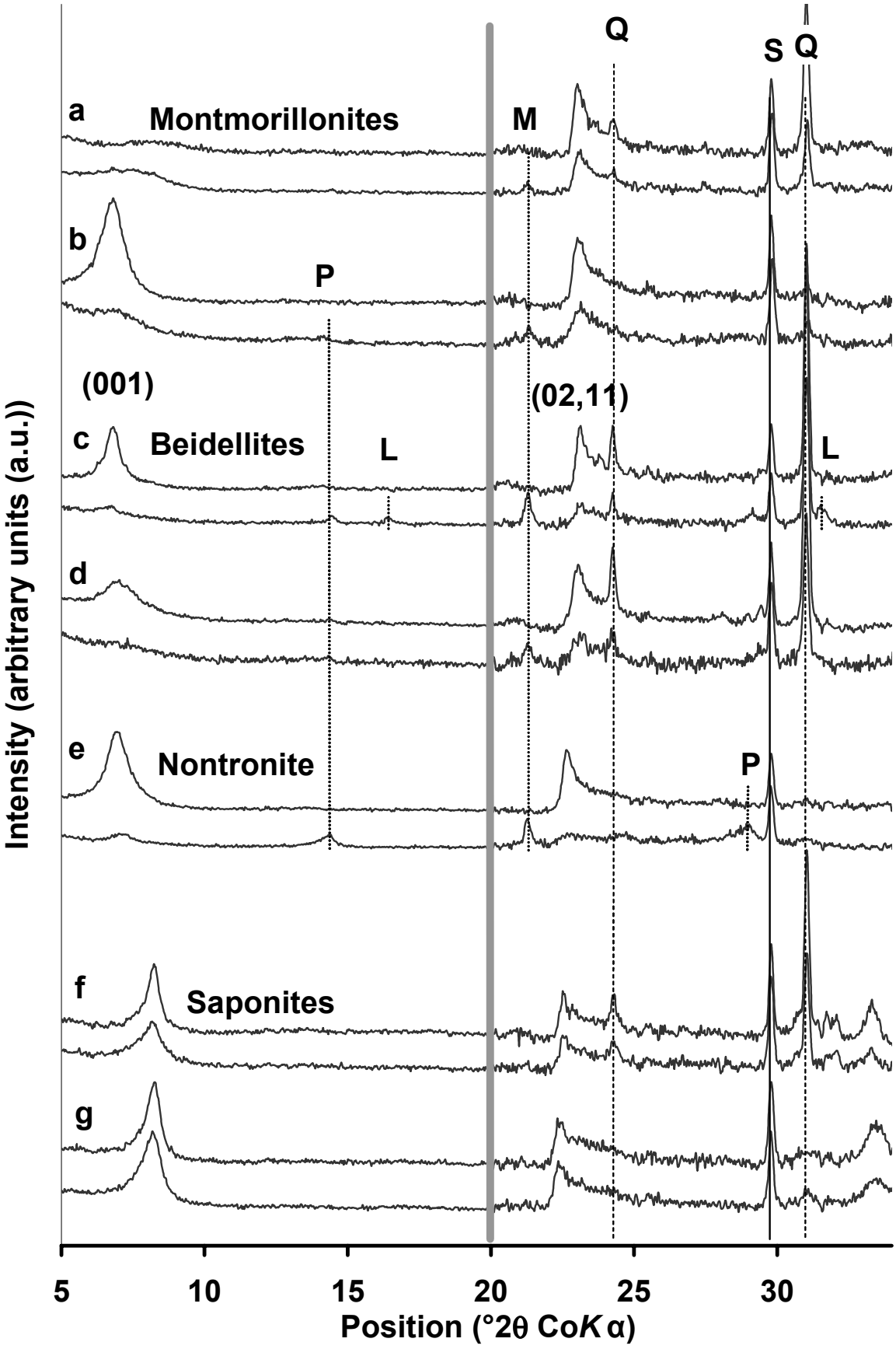
Q
S
Q
a
Montmorillonites
M
b
P
(001)
(02,11)
c
Beidellites
L
L
d
e
Nontronite
P
f
Saponites
g
Intensity (arbitrary units (a.u.))
5
10
15
20
25
30
Position (°2θ CoKα)

Figure 2 :

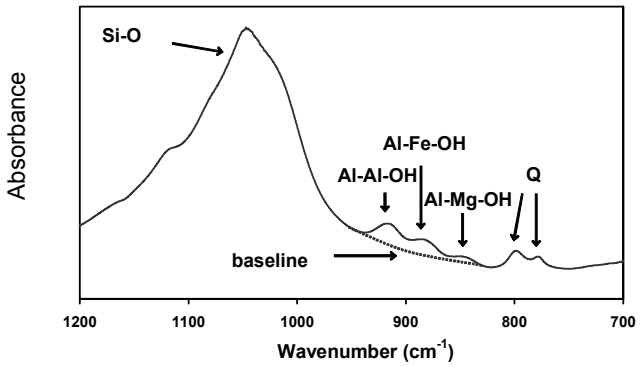
Si-O
Al-Fe-OH
Al-Al-OH
Al-Mg-OH
Q
baseline
Absorbance
1200
1100
1000
900
800
700
Wavenumber (cm-1)

a

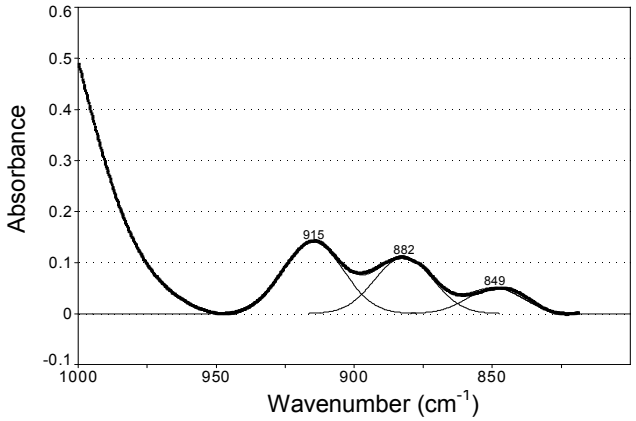
Absorbance
0.6
0.5
0.4
0.3
0.2
0.1
0
-0.1
915
882
849
1000
950
900
850
Wavenumber (cm-1)

b

Figure 3 :

a

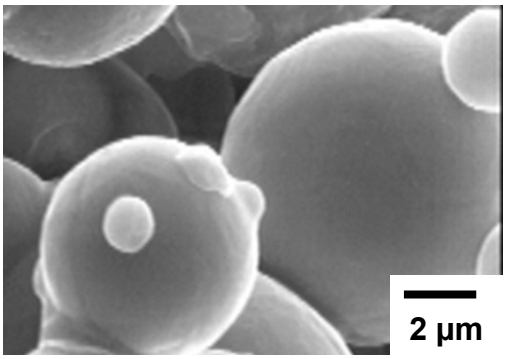

b

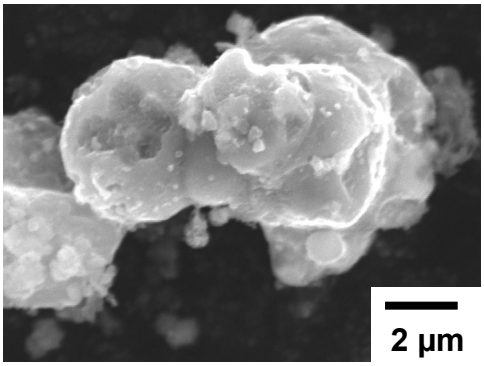

c

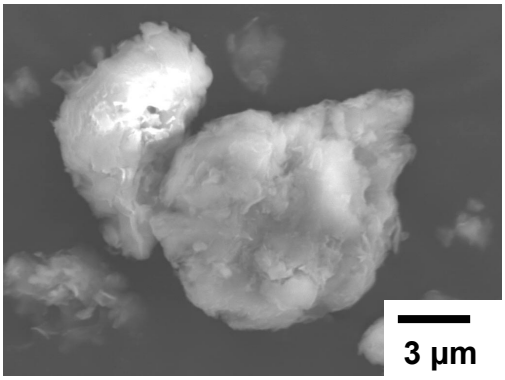

d

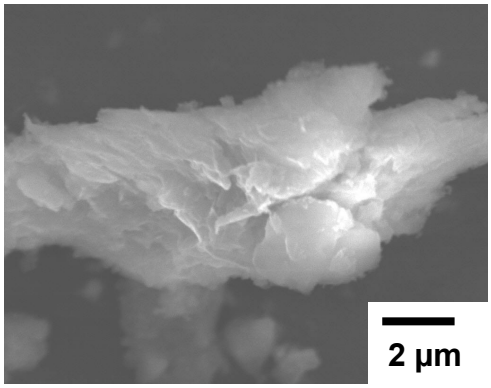

e

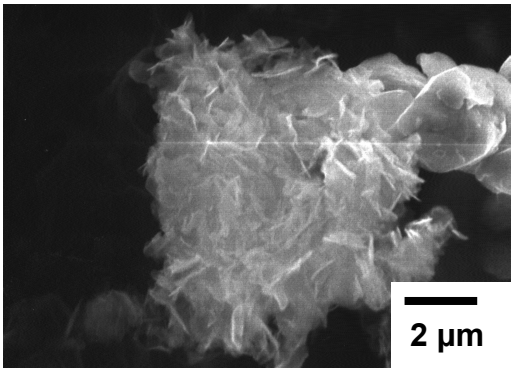

f

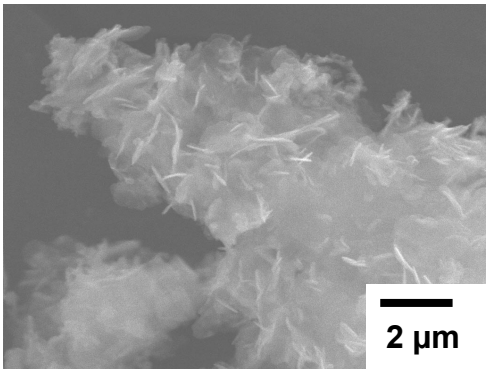

g

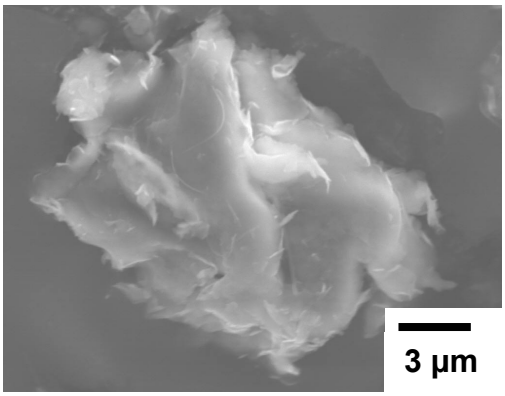

h

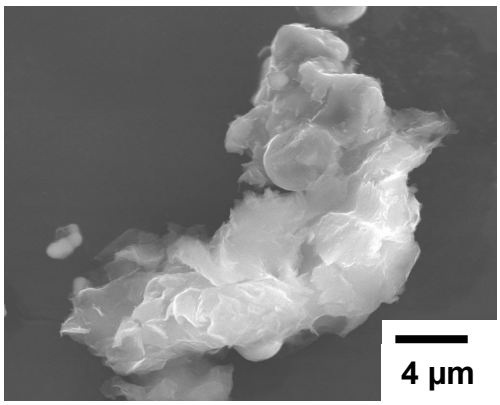

Figure 4 :

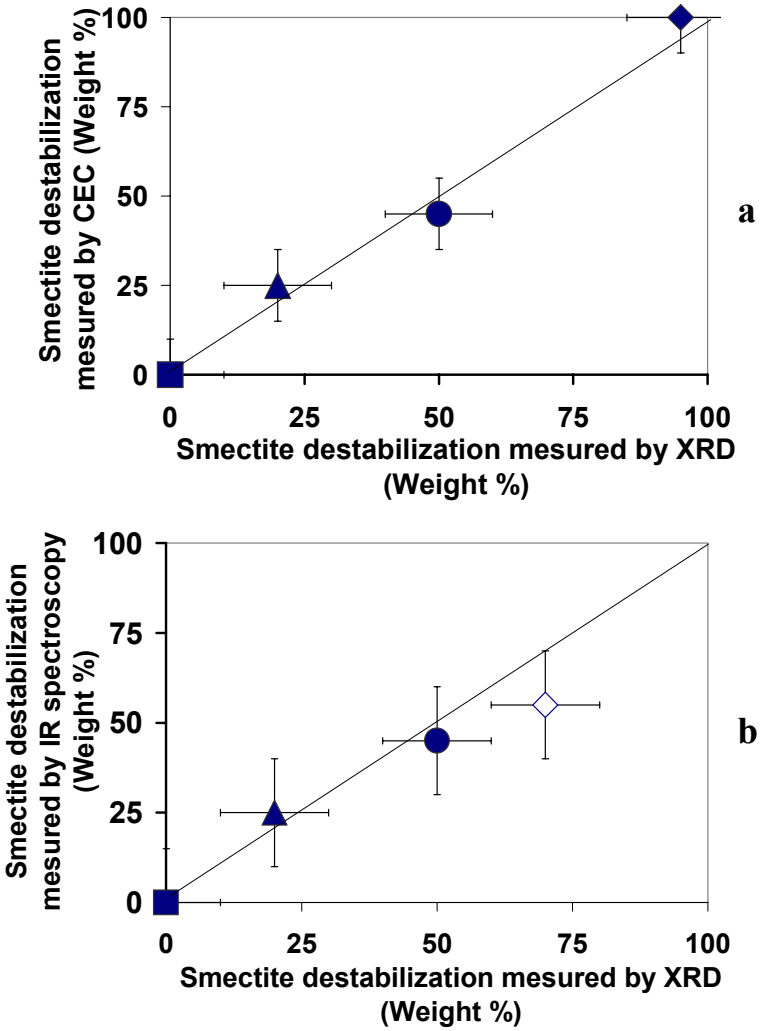
Smectite destabilization mesured by CEC (Weight %)
100
75
50
25
0
0
25
50
75
100
Smectite destabilization mesured by XRD (Weight %)
a
Smectite destabilization mesured by IR spectroscopy (Weight %)
100
75
50
25
0
0
25
50
75
100
Smectite destabilization mesured by XRD (Weight %)
b

Figure 5 :

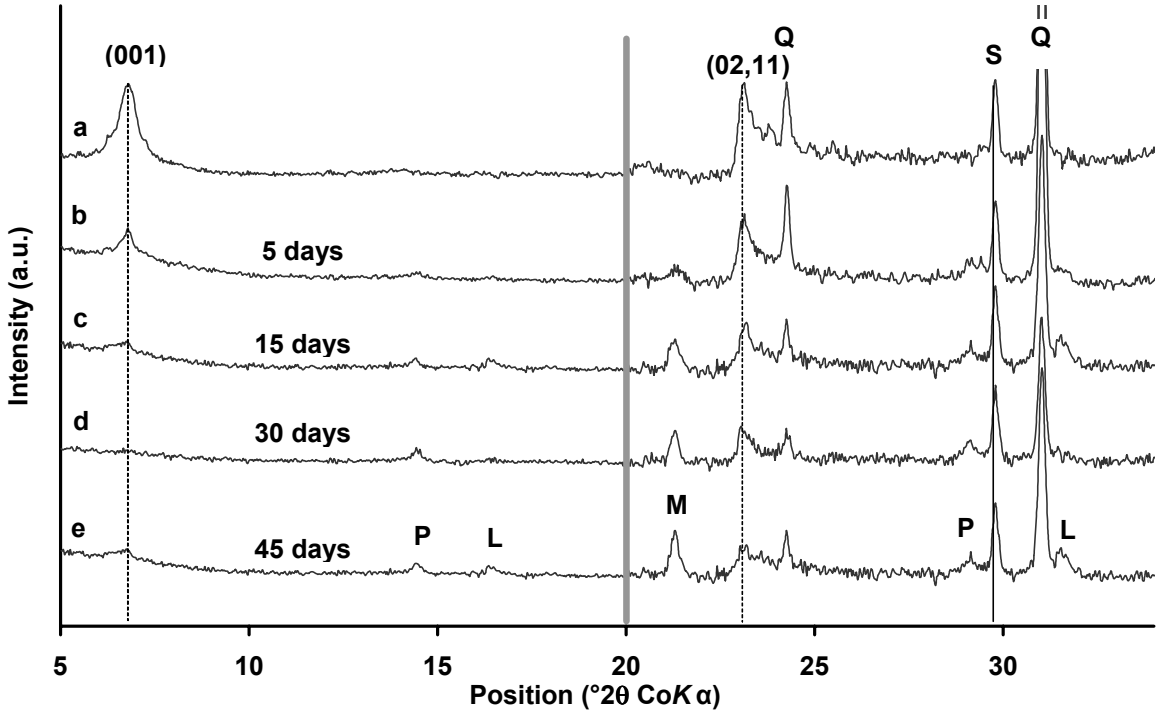

Figure 6 :

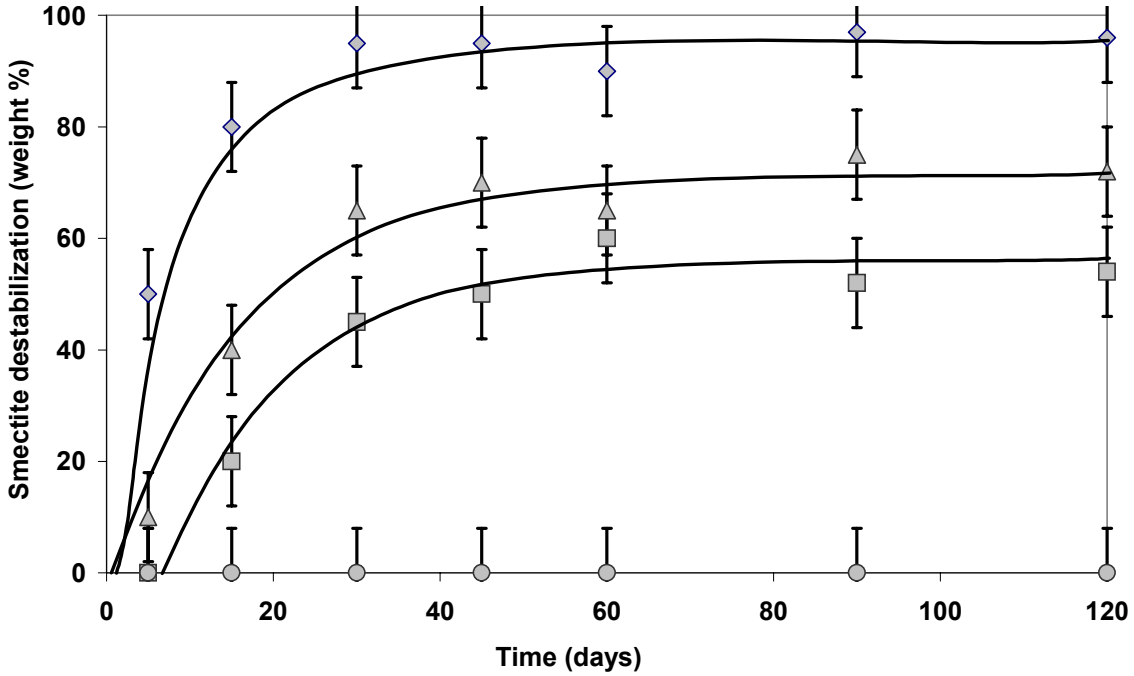

Figure 7 :

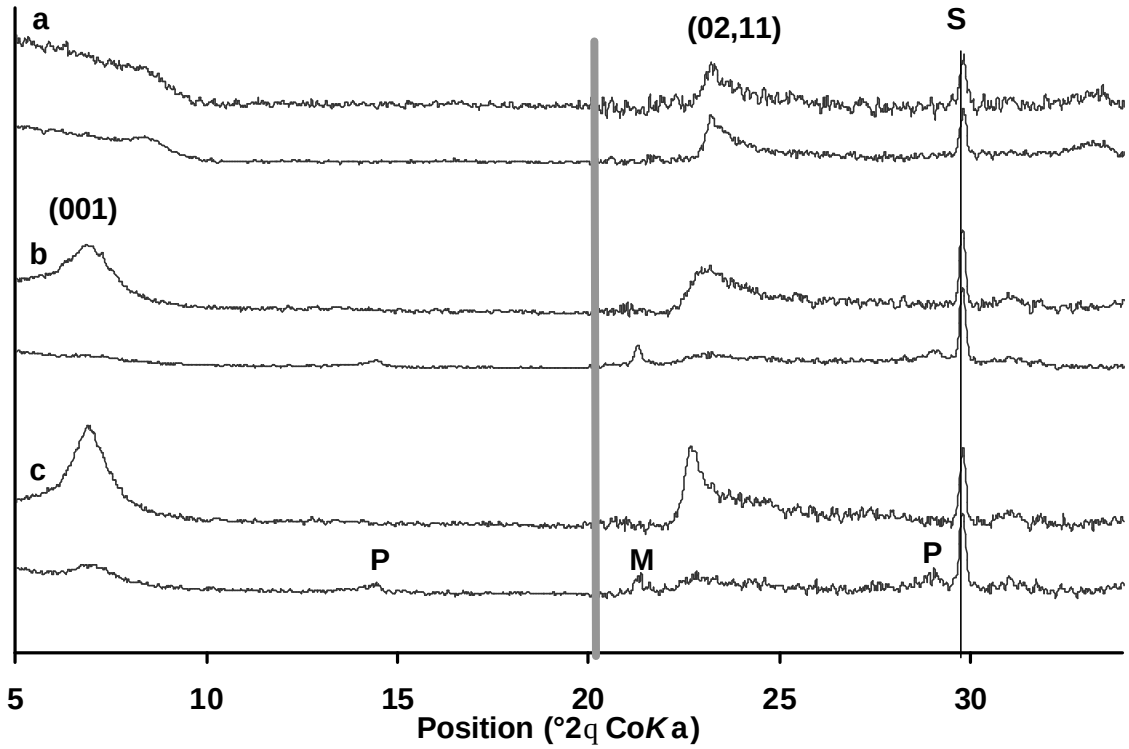

Figure 8 :

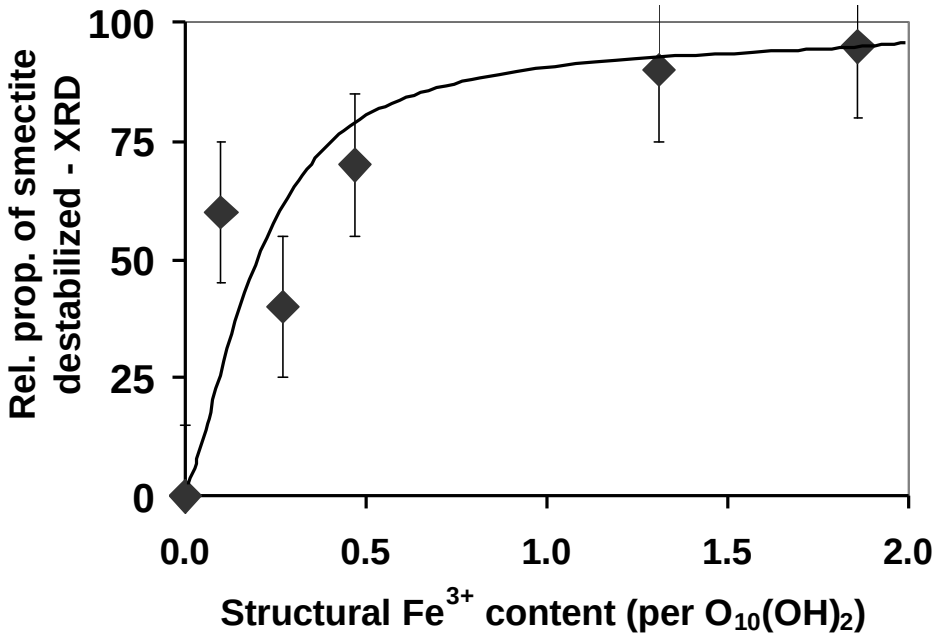

Figure 9 :

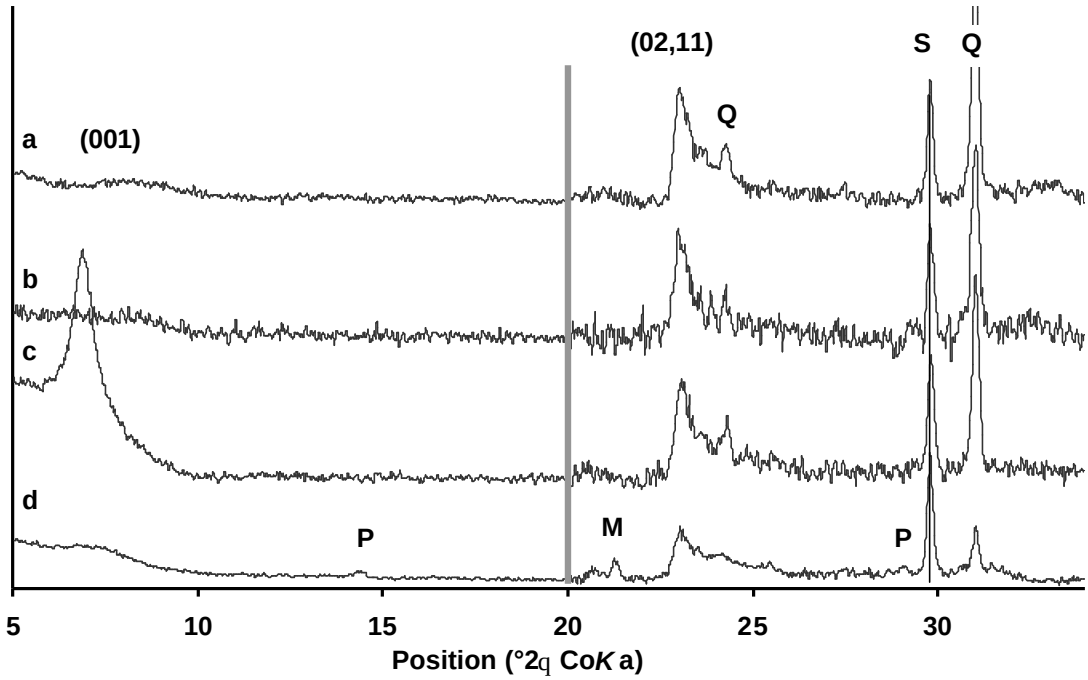

Figure 10 :

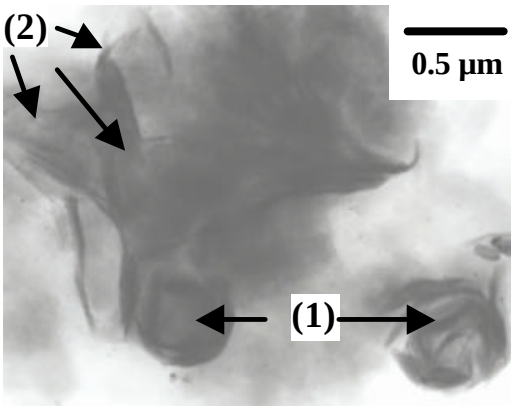

Figure 11

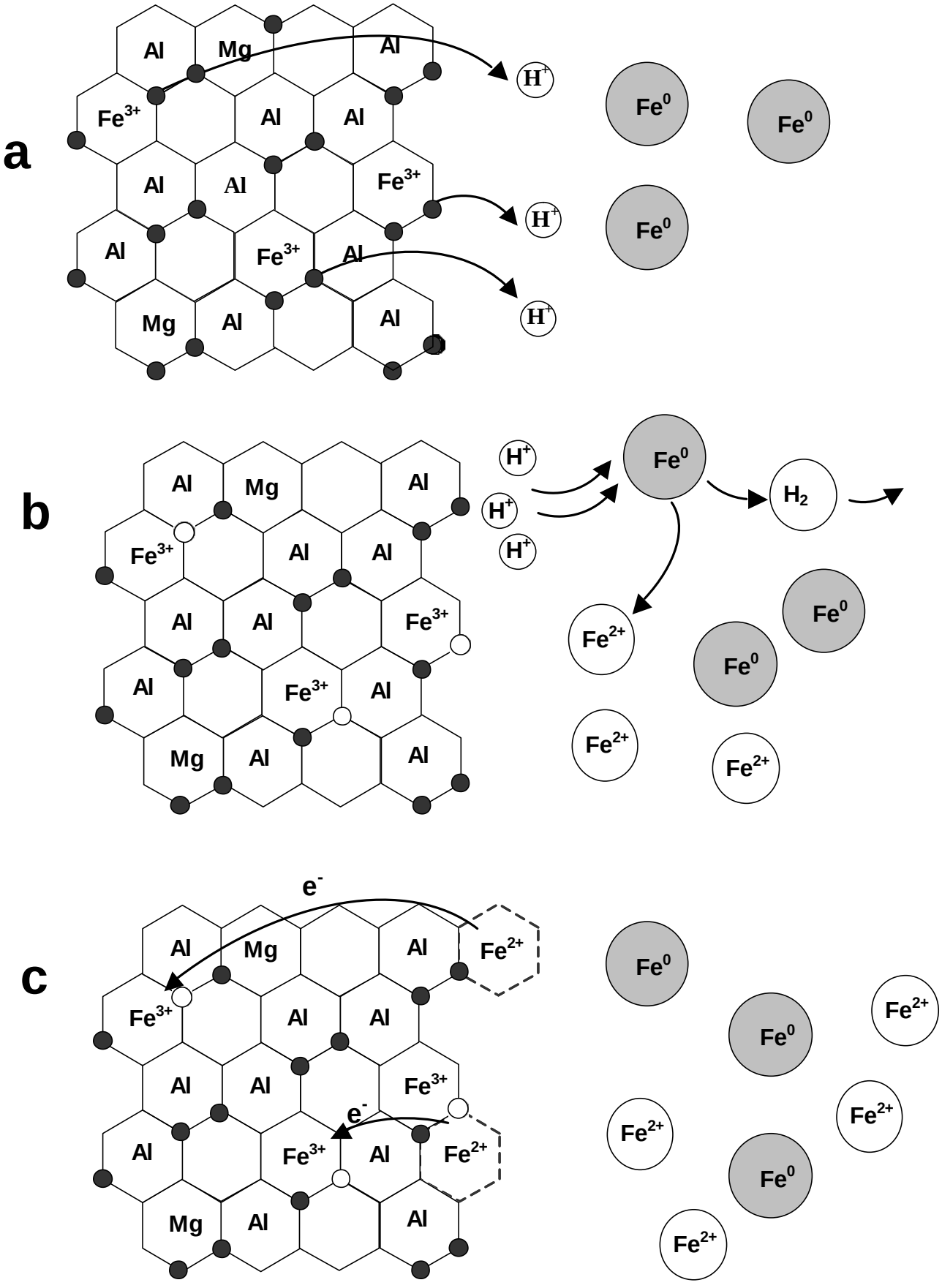
a
Al
Mg
Al
Fe3+
Al
Al
Al
Al
Fe3+
Al
Fe3+
Al
Mg
Al
Al
H+
H+
H+
Fe0
Fe0
Fe0
b
Al
Mg
Al
Fe3+
Al
Al
Al
Al
Fe3+
Al
Fe3+
Al
Mg
Al
Al
H+
H+
H+
Fe0
H2
Fe2+
Fe0
Fe0
Fe2+
Fe2+
c
e-
Al
Mg
Al
Fe2+
Fe3+
Al
Al
Al
Al
Fe3+
e-
Al
Fe3+
Al
Fe2+
Mg
Al
Al
Fe0
Fe0
Fe2+
Fe2+
Fe0
Fe2+

d

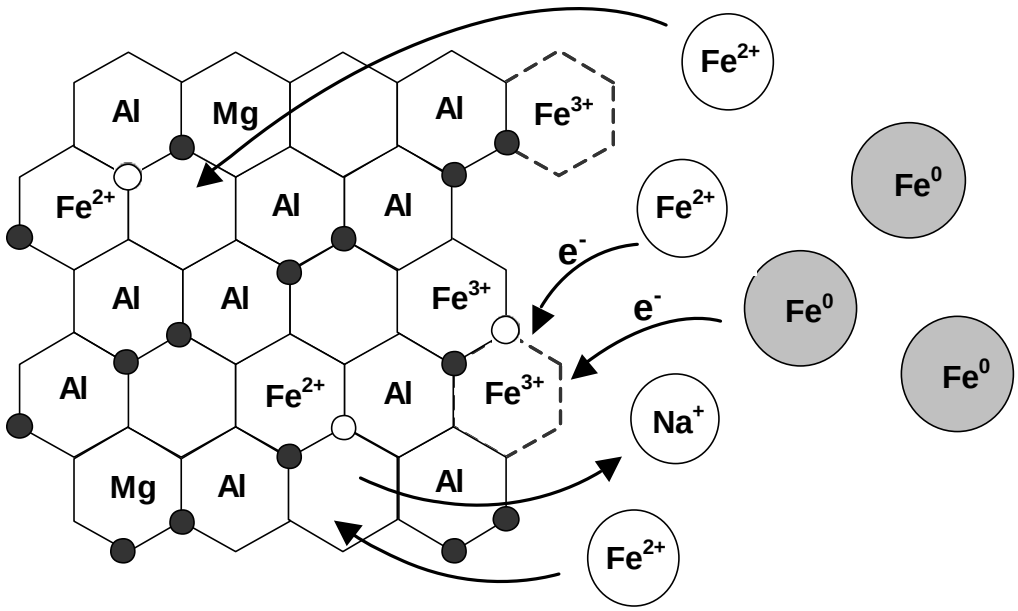
Al
Mg
Al
Fe3+
Fe2+
Al
Al
Fe2+
e-
Al
Al
Fe3+
e-
Al
Fe2+
Al
Fe3+
Na+
Mg
Al
Al
Fe2+
Fe2+
Fe0
Fe0
Fe0

e

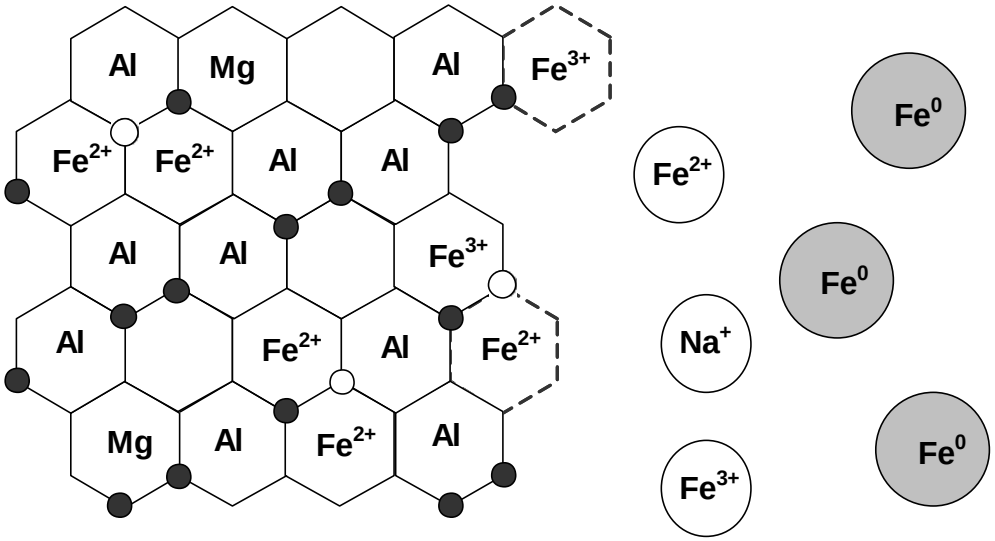
Al
Mg
Al
Fe3+
Fe0
Fe2+
Fe2+
Al
Al
Fe2+
Al
Al
Fe3+
Fe0
Al
Fe2+
Al
Fe2+
Na+
Mg
Al
Fe2+
Al
Fe0
Fe3+